Thesis

Modeling of Atmospherically Important Vapor-to-Particle Reactions

Submitted by

Bahaudin Hashmi

Department of Mathematics

In partial fulfillment of the requirements

For the Degree of Master of Science

Colorado State University

Fort Collins, Colorado

Summer 2014

Master's Committee:

Advisor: Patrick Shipman
Co-Advisor: Jiangguo Liu

Stephen Thompson

Abstract

Modeling of Atmospherically Important Vapor-to-Particle Reactions

Liesegang ring formation is a special type of chemical pattern formation in which a spatial order is formed by density fluctuations of a weakly soluble salt. The Vapor-to-Particle nucleation process that is believed to produce these Liesegang rings is theorized to be the cause of mini-tornadoes and mini-hurricanes developed in a lab. In this thesis, we develop a one-dimensional finite element scheme for modeling laboratory experiments in which ammonia and hydrogen chloride vapor sources are presented to either end of the tubes. In these experiments, a reaction zone develops and propagates along the tube. Both numerical simulations and the laboratory experiments find an increasing amplitude of oscillations at the reaction front.

Table of Contents

CHAPTER 1

Introduction

1.1. Background on Liesegang Rings

Liesegang ring formation is a special type of chemical pattern formation in which the spatial order is formed by density fluctuations of a weakly soluble salt. The phenomenon was first noticed in 1896 by German chemist Raphael E. Liesegang. Liesegang noted the patterns when he dropped a solution of silver nitrate on to a thin layer of gel containing potassium dichromate. After some time, sharp concentric rings of insoluble precipitate were formed at regular intervals. Since then, this phenomenon was observed in many other different systems and sparked the curiosity of chemists [1]. A proposed mechanism for this type of formation was first given by Wilhelm Ostwald and was based on the concept of repetitive supersaturation in the system.

In analytical chemistry, this can be observed in the reaction between silver nitrate ($AgNO_3$) and potassium dichromate ($K_2Cr_2O_7$) and between ammonia ($NH_3(g)$) and hydrogen chloride ($HCL(g)$).In geology, Liesegang ring formation is observed in sedimentary

Figure 1.1. Liesegang ring formation in $HCl - NH_3$ Lab Experiment

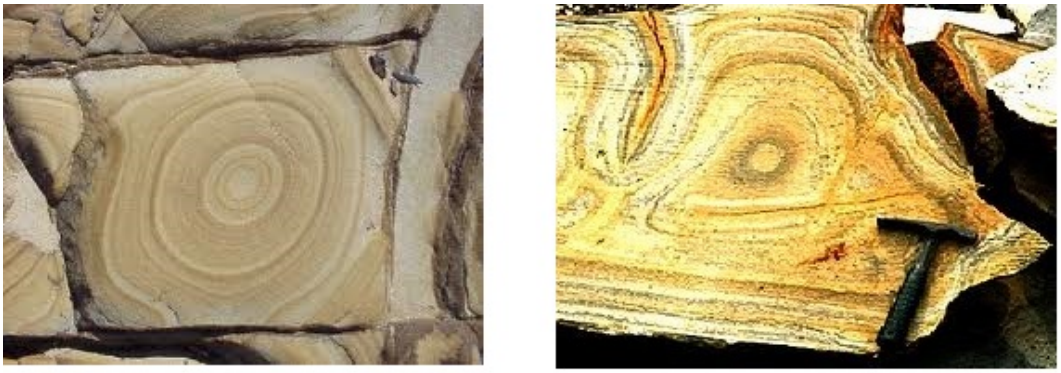

FIGURE 1.2. Liesegang Ring Formation in Geology

rocks. It is also believed that the nucleation process that causes Liesegang ring formation, which will be discussed shortly, is also responsible for stone formation in kidneys.

1.2. Vapor-to-Particle Liesegang Ring Formation

In this paper we are particularly interested in the Vapor-to-Particle Liesegang ring formation. To be more precise we will be analyzing the formation of the precipitate ammonium chloride (NH_4Cl) from the reaction between ammonia ($NH_3(g)$) and hydrogen cholride ($HCl(g)$). In this paper we use a lot of the information given in [2] and in Timothy Lenczycki's master thesis [3]. The main purpose of this paper is to provide and analyze a mathematical model to compare with Timothy Lenczycki's experimental results [3].

The Vapor-to-Particle system is of particular interest because this system can lead to extreme scenarios under particular conditions. This particular system of ammonia and hydrogen chloride produced mini-tornadoes and mini-hurricanes in lab settings. Our aim is to further enhance our understanding of the phase transitions in this process so that we can introduce more dynamics of phase changes and reactions and transport such results to chemistry, engineering and mathematics of course. In this paper we mathematically model the reaction between ammonia (NH_3) and hydrogen chloride ($HCL(g)$). This chemical reaction

is particular interesting for the recurring precipitary rings that form. The reaction which produces these rings undergo a process of nucleation. This process converts the gaseous ammonium chloride that initially forms, to ammonium chloride in solid form. The purpose of this paper is to generate a mathematical model and to use a finite element scheme to numerically solve the model equations which eventually would help us in predicting the position, time and other qualitative and quantitative results.

1.3. Outline

To explain this entire process and the results of our findings we divide our paper into four sections. In the first, after discussing some of the theories believed to be governing this process of nucleation and ring formation, we discuss the various experiments conducted in the lab and some of the interesting results obtained. The next section will explain the mathematical model theorized to govern this reaction. We present the Partial Differential System and the various modifications to the Global Right-Hand side to mimic the lab experiments discussed in Section 2. We then discuss the various numerical techniques used to solve the Partial differential System. We show the various Right-Hand side equations used to mimic the threshold kinetics as expressed in [4]. Our final chapter discusses the various results we achieved using different techniques and how they correlate or don't correlate to certain results achieved or expected in experiments conducted in the lab.

CHAPTER 2

Vapor-to-Particle Reaction: Mechanisms and Experiments

2.1. Kinetics and Mechanism

Our experiments are based on the reaction between ammonia (NH_3) and hydrogen chloride (HCl). Ammonia and hydrogen chloride are both in the gaseous state when they are reacted together in a tube. In the process, there is a phase transformation in the state of the product ammonium chloride from a gaseous to a solid state.

$$NH_3(g) + HCl(g) \longrightarrow NH_4CL(g)$$

$$NH_4CL(g) \longrightarrow NH_4CL(s)$$

However, the entire process is a lot more complicated than in the two lines mentioned before. According to various papers[5, 6] the process involves a lot more steps before the actual precipitate is formed. The first step is a fast, water-catalyzed proton transfer;

$$\text{(1)} \qquad \mathrm{NH_{3(g)} + HCl_{(g)} \overset{H_2O}{\rightleftharpoons} {NH_4}^+Cl^- \cdot nH_2O}, \qquad (n = 2, 3, 4).$$

This transfer produces an ammonium ion NH_4^+ and a Cl^-. This process varies differently under anhydrous condition then when the solution is hydrated [5, 6]. The chloride ions then redistribute their charge which then acts as a catalyst before the addition of hydrogen chloride and ammonia monomers. The whole process can be given by the following equations;

$$
\begin{aligned}
&\mathrm{Cl^-} + \mathrm{HCl} \longrightarrow \mathrm{Cl^-} \cdot \mathrm{HCl} \\
&\mathrm{Cl^-} \cdot \mathrm{HCl} + \mathrm{NH_3} \longrightarrow \mathrm{Cl^-} \cdot \mathrm{NH_4Cl} \\
&\mathrm{Cl^-} \cdot \mathrm{NH_4Cl} + \mathrm{HCl} \longrightarrow \mathrm{Cl^-} \cdot \mathrm{HCl} \cdot \mathrm{NH_4Cl} \\
&\mathrm{Cl^-} \cdot \mathrm{HCl} \cdot \mathrm{NH_4Cl} + \mathrm{NH_3} \longrightarrow \mathrm{Cl^-} \cdot (\mathrm{NH_4Cl})_2 \\
&\qquad\vdots \qquad\qquad\qquad\vdots \\
&\mathrm{Cl^-} \cdot (\mathrm{NH_4Cl})_\mathrm{n} + \mathrm{HCl} \longrightarrow \mathrm{Cl^-} \cdot \mathrm{HCl} \cdot (\mathrm{NH_4Cl})_\mathrm{n} \\
&\mathrm{Cl^-} \cdot \mathrm{HCl} \cdot (\mathrm{NH_4Cl})_\mathrm{n} + \mathrm{NH_3} \longrightarrow \mathrm{Cl^-} \cdot (\mathrm{NH_4Cl})_{\mathrm{n}+1}
\end{aligned}
\tag{2}
$$

The kinetics of other reactions of aerosol formation are not as well understood as that of ammonium chloride [2]. According to [2] "the stepwise addition of ammonia and hydrogen chloride proposed in Equation 2 is similar to a mechanism recently proposed for the formation of ammonium sulfate based on experiments in CERN [7]".

To understand this mechanism in a more simple way let us consider an experiment set up by Fig. 2.3(a). We introduce ammonia and hydrogen chloride at either end of the tube with particular concentration values. Both of the reactants diffuse through the tube and form what we term a reaction front at the point where the two reactants meet. What is observed in the lab and explained by [3], dust particles inside the tube act as catalysts for the formation of precipitate at the reaction front once the ammonium chloride vapor is formed. This is known as heterogeneous nucleation (see Section 2.2), where the process of the vapor-to-particle phase transformation is assisted by a 'foreign' object. After the dust particles are removed due to this phase transformation, there is a region inside the tube at the reaction front where the concentration of ammonium chloride is building up . This is the starting point of our mathematical simulation. We ignore the existence of the dust particles

and assume that no form of heterogeneous nucleation takes place at the beginning of the experiment. How the reaction progresses from there is explained in Section 2.2.

2.2. Nucleation and Growth

Understanding the process of nucleation and growth is central to understanding the formation of Liesegang rings in ammonia and hydrogen chloride reaction. Ammonium chloride is initially formed in a gaseous state. Once the concentration of ammonium chloride reaches a critical level, the vapor ammonium chloride nucleates to a solid state.

$$NH_4CL(g) \longrightarrow NH_4CL(s)$$

To understand this apparently very simple reaction, we can refer to Fig. 2.1(B). 'J' is the nucleation rate (nuclei $dm^{-3}\ s^{-1}$) and 'S' is the supersaturation ratio ($\frac{C}{C_o}$). From Fig. 2.1(B) we can see the rate of nucleation increases at relatively lower rate for values before S_{crit}. But once S is above S_{crit}, the rate of nucleation drastically increases with a very slight increase in the supersaturation value. This is the point where homogeneous nucleation takes place. Homogeneous nucleation by definition is the formation of precipitate without the existence of previously formed precipitate. It is at this point we can see the first inklings of a 'ring' forming. In order for the ring to form there is a drastic drop in 'S' as 'C' is needed to form the precipitate. Once homogeneous nucleation takes place, the newly formed precipitate of ammonium chloride acts as a catalyst for further nucleation. This form of precipitation formation is known as Heterogeneous nucleation. The concentration threshold required for further nucleation drops drastically once homogeneous nucleation takes place. The link between precipitate and the threshold requirement for the nucleation is given in Fig. 2.1(A). It is estimated according to [2] that homogeneous threshold concentration for the ammonium

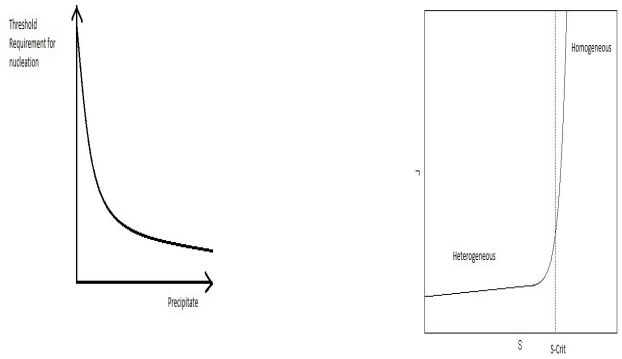

(A) (B)

FIGURE 2.1. Mechanics of nucleation

chloride reaction is of the order $10^{-2}g/cm^3$. The threshold concentration however does not go below an order of $10^{-3}g/cm^3$. So although the marginal affect of the precipitate for small amounts is very high on the concentration threshold, its affect decreases as more precipitate forms.

This entire nucleation process leads to a 'pulsating' effect at the reaction front. The monomer ammonium chloride forms at the reaction front which leads to the formation of the precipitate ammonium chloride. This formation leads to a drastic drop in the concentration of the monomer. As soon as the reaction front moves, the original state achieves an equilibrium and that entire process takes place at a more advanced position in the tube in a similar way. As a result, we predict and see in our simulations as described in Section 5, that the system is extremely sensitive to the following three quantities:

(1) Reaction Front Speed.

(2) Threshold Value.

(3) Reaction rate between Ammonia and Hydrogen Chloride.

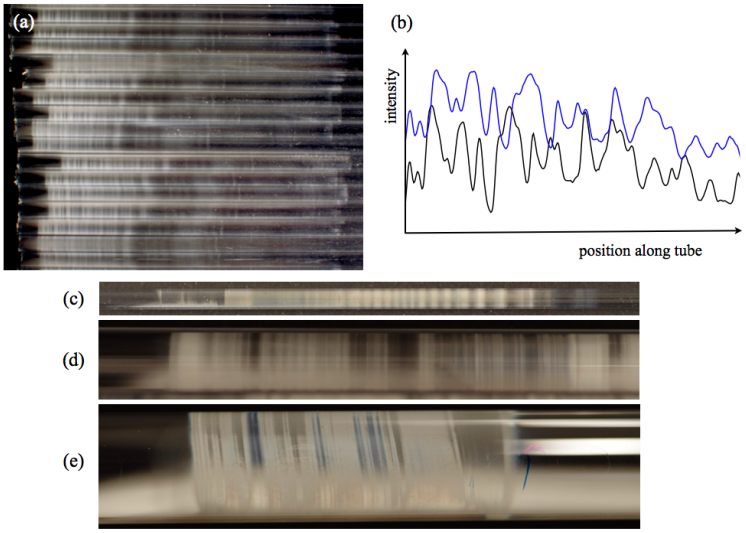

FIGURE 2.2. Liesegang rings produced by counter-diffusional HCl/NH_3 systems in (a) 10 cm / 0.2 cm I.D. bundled glass melting point tubes, (c) a 10 cm / 0.2 cm I.D. glass melting point tube (this is a rare example of a pattern in a vapor-to-particle system in which the rings nearly obey a Morse-Pierce scaling law), (d) a 120 cm/ 1 cm I.D. glass tube, and (e) a 120 cm/ 2 cm I.D. glass tube. A plot of the intensity of the pattern in two of the tubes in (a) is shown in (b). The patterns in these example were produced from right to left with the NH_3 vapor source at the right, and the HCl vapor source at the left.

2.3. EXPERIMENTS

2.3.1. COUNTER-DIFFUSIONAL EXPERIMENT. In a counter-diffusional experiment, the tube in which the reaction is to be conducted does not contain any of the reactants. In other words, the entire tube is devoid of either ammonia and hydrogen chloride at the start of the experiment(refer to Fig. 2.3). For the reaction to take place, both the reactants are introduced at the ends of the tube with ammonia at one end and hydrogen chloride at the other and through diffusion react at some point within the tube. The precise technique of conducting these experiments is described generously in [2].

The experiments were carried out for varying lengths and diameters of the tube. For our mathematical simulations, we consider this a one dimensional system. So as far as correlating our results with what was obtained from the lab, the analysis will be best with the experiments where the diameter of the tube is the smallest.

In the paper [2], some general analysis were given for the counter-diffusional experiments. For example, if the concentration was lower the 'bands' of precipitate were longer at lower concentrations than at higher concentrations. Because of the nature of the chemical reaction, a lot of energy is released in the formation of the precipitate and that causes convection currents within the tube. These convection currents have produced very interesting result in lab experiments. Fig. 2.3(d) shows a lab experiment which produced micro-tornadoes. Similarly Fig. 2.3(e) show the production of micro-geysers produced in a lab experiment. As far as the analysis of these aforementioned scenarios goes, we have ignored them in the development of our mathematical model, but would be nice to include the affect of convection currents in further, more comprehensive models.

Liesegang ring formation in counter-diffusional experiments are generally not regularly observed. For our simulations, more data is available for saturated-vapor models. It is still not clear what exactly causes the Liesegang ring formation in counter-diffusional experiments. Theories vary from homogeneous and heterogeneous nucleation to even post nucleation processes. Hopefully our mathematical analysis will be able to shed some light on this process.

Fig. 2.2 illustrates the results of some actual counter-diffusional experiments in the lab. Fig. 2.2(b) is of particular interest because that is the only means through which we can correlate our simulations with the empirical data from [3].

2.3.2. Saturated-Vapor Experiments. In saturated-vapor experiments, one of the reactants is diffused into the tube that already contains an equilibrated state of the other reactant of known concentration (see Fig. 2.3(b)). In the experiments done in the lab [3], the 20 cm tube is saturated with hydrogen chloride vapor and ammonia is allowed to diffuse into it. In contrast to the counter-diffusional experiment, precipitate immediately forms

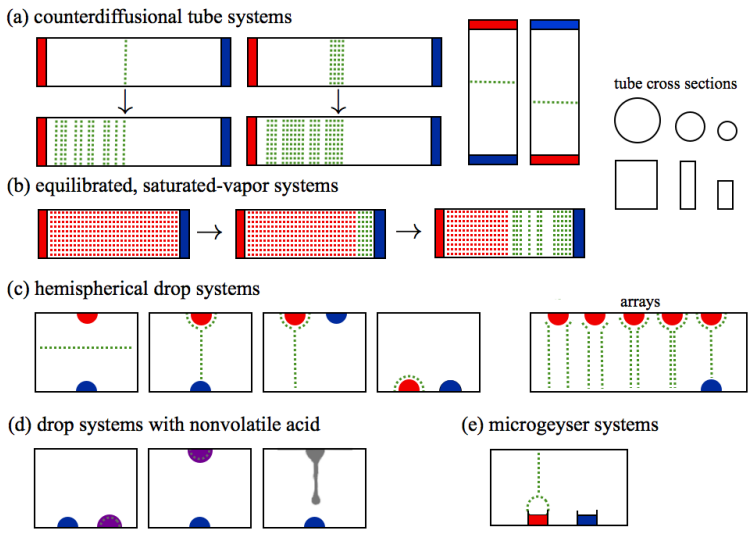

FIGURE 2.3. Configurations of reactant source (red: HCl, blue: NH_3, purple: non-volatile acid) configurations and product exhaust (green). (a) A counter-diffusional tube experiments, (b) Saturated-vapor tube (discussed in Section 2.3.2, and (c) hemispherical drop experiments, (d) drop systems with a nonvolatile acid, and (e) micro-geyser systems in.

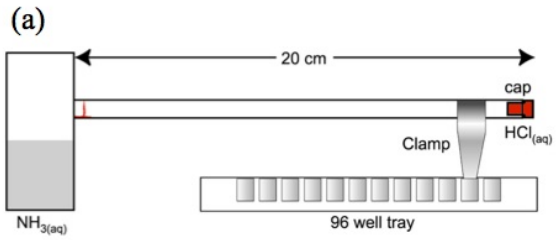

FIGURE 2.4. Saturated Vapor tube experiment.

and can be seen 'progressing' along the length of the tube. Around about one third of the length of the 20 cm tube, oscillatory behavior is observed at the reaction front. Because the progression of the monomer ammonium chloride cannot be analyzed by video , these oscillations correspond to the precipitate. By oscillations, we mean different levels of precipitate being deposited at the reaction front. Although, according to [3] the 'oscillations' happen one-third of the distance along the tube, we can see in our mathematical simulations that these oscillations are immediately occurring in the system but perhaps only become visibly

apparent as the frequency of the precipitate deposits decreases. This oscillatory behavior is caught on video. As the reaction front slows down the frequency of the oscillation slows down and the amplitude increases. Eventually, according to [2] the oscillations become 'irregular and irreproducible', primarily because of the reaction front's slowing down a considerable degree.

CHAPTER 3

Mathematical Model

3.1. A Model of Partial Differential Equations

For our mathematical model [2], the chemical reaction is mapped by a system of parabolic differential equations. Ignoring the complicated processes expressed in Section 2.1, we reduce our system to the following chemical process:

$$a_{(g)} + b_{(g)} \longrightarrow c_{(g)}$$

$$c_{(g)} \longrightarrow d_{(s)}$$

where a represents the concentration of hydrogen chloride, b represents the concentration of ammonia, c represents the concentration of the vapor ammonium chloride whereas d represents the precipitate ammonium chloride. All units of concentration are given in g/cm^3. D_a,D_b, D_c represent the diffusion coefficients of hydrogen chloride, ammonia and ammonium chloride, respectively. The mathematical equation modeling the system is as follows:

$$\text{(3)} \qquad \begin{cases} \frac{\partial a}{\partial t} &= D_a \frac{\partial^2 a}{\partial x^2} - kab - f_1(a,b,c,d) \\ \frac{\partial b}{\partial t} &= D_b \frac{\partial^2 b}{\partial x^2} - kab - f_1(a,b,c,d) \\ \frac{\partial c}{\partial t} &= D_c \frac{\partial^2 c}{\partial x^2} + kab - f_2(a,b,c,d) \\ \frac{\partial d}{\partial t} &= f_2(a,b,c,d) \end{cases}$$

where $a(x,t)$,$b(x,t)$ and $c(x,t)$ are functions of space (x=distance along the tube) and time(t). As the precipitate is a solid and it does not diffuse, we consider it to be just an ordinary differential equation.

3.2. Threshold Kinetics

The real debate in the modeling of this problem is in determining the appropriate Right-Hand side function $f_i(a,b,c,d)\ \forall\ i = 1,2$ for the precipitate d. The nucleation process is based on threshold kinetics. The precipitate does not form unless the concentration of the product is above a certain threshold value. In reality the threshold is also affected by the concentration of the reactants however, in our case we ignore it. Hence, $f_1(a,b,c,d) = 0$. The threshold function is given by $g(d)$. The qualitative behavior of $g(d)$ is similar to that shown in Fig. 2.1(A). As more d is produced, the threshold requirement for its formation '$g(d)$' is reduced. According to Keller and Rubinow [4], the threshold kinetics for $f_2(a,b,c,d)$ is given by the following equation:

$$f_2(a,b,c,d) = \begin{cases} 0 & \text{if } c \le g(d), \\ c - g(d) & \text{if } c > g(d). \end{cases} \tag{4}$$

where,

$$g(d) = \begin{cases} c_s > 0 & \text{for } d > 0, \\ c_{ss} > c_s & \text{for } d = 0. \end{cases} \tag{5}$$

Equation 5 mathematically demonstrates the difference between homogeneous and heterogeneous nucleation. c_{ss} is a threshold requirement for the concentration level of 'c' for

homogeneous nucleation to take place. c_{ss} is generally believed to be of order 10^{-2}. c_s represents the concentration requirement for heterogeneous nucleation and is generally believed to be of the order of 10^{-3} [2]. Unlike c_{ss}, c_s is not a constant value but a function of 'd'. As more precipitate increases , c_s decreases.

3.3. Boundary Conditions

Apart from trying to determine the appropriate threshold function representing Equation 4, for our simulations we will vary a few parameters. Amongst those, different boundary and initial conditions play an important role in simulating different classes of experiments. Despite tubes being three dimensional objects, we assume our system to be in one dimension. So for our simulations, our boundary conditions are concentrations at the extreme end points of the one dimensional tube. For this counter-diffusional experiment, the boundary conditions are given by equation 6.

$$\begin{cases} a(0,t) = a_o, & b(0,t) = b_o \\ \frac{\partial a}{\partial x}(L,t) = 0, & \frac{\partial b}{\partial x}(0,t) = 0 \\ \frac{\partial c}{\partial x}(0,t) = 0, & \frac{\partial c}{\partial x}(L,t) = 0 \\ \frac{\partial d}{\partial x}(0,t) = 0, & \frac{\partial d}{\partial x}(L,t) = 0, \end{cases} \tag{6}$$

The boundary conditions are qualitatively the same for the two experiments i.e. a_0 and b_0 are both non-negative values in the counter-diffusional model and the saturated-vapor model.

3.4. Initial Conditions

The initial conditions however, are different in both the experiments. In the case of the counter-diffusional experiment $a_1 = 0$ and $b_1 = 0$. In the saturated-vapor model, we choose the initial condition of one of the two reactants to be greater than zero. In the lab experiments conducted by Tim Lenczycki [3], the concentration of hydrogen chloride was greater than zero at the beginning of the experiment. In our simulations, we take the liberty to model cases where either ammonia or hydrogen chloride have an initial concentration greater than zero at the start of the simulation.

$$\begin{cases} a(x,0) &= a_1 \\ b(x,0) &= b_1 \\ c(x,0) &= 0 \\ d(x,0) &= 0 \end{cases} \tag{7}$$

Once the PDE system is set, up we discuss various solution techniques in Chapter 4.

CHAPTER 4

Numerical Techniques

To solve the mathematical model represented by Equation 3, a finite element scheme for a one dimensional parabolic system is developed. First, however we decouple the reactants a (hydrogen chloride) and b (ammonia) from the model. This is a simplification of the model as both the reactants are believed to affect the heterogeneous nucleation process. After solving for the reactants our initial model given by Equation 3 can be reduced to Equation 8, where a and b are solved for beforehand using the MATLAB PDE solver.

$$\begin{cases} \frac{\partial c}{\partial t} & = D_c \frac{\partial^2 c}{\partial x^2} + kab - f(c,d) \\ \frac{\partial d}{\partial t} & = \qquad\qquad\qquad f(c,d) \end{cases} \tag{8}$$

4.1. Assembling Of Matrices

In order to solve Equation 8, the spatial domain is partitioned into a uniform mesh with mesh size 'h' intervals of uniform length. We use P_1 finite elements for approximation. The Element Stiffness Matrix is $\mathrm{A}= \begin{bmatrix} \frac{1}{h} & \frac{-1}{h} \\ \frac{-1}{h} & \frac{1}{h} \end{bmatrix}$,

where 'h' is the length of one element or subinterval in the spatial domain. We assemble these Element Stiffness Matrices into Global Stiffness Matrix. Because of the uniformity of the size of the interval, it is relatively easy to obtain the Global Stiffness Matrix. This produces a tri-diagonal matrix as follows;

$$\text{B}=\begin{bmatrix} \frac{1}{h} & \frac{-1}{h} & 0 & 0 & \dots \\ \frac{-1}{h} & \frac{2}{h} & \frac{-1}{h} & 0 & \dots \\ 0 & \frac{-1}{h} & \frac{2}{h} & \frac{-1}{h} & \dots \\ 0 & 0 & \frac{-1}{h} & \frac{2}{h} & \dots \\ \vdots & \vdots & \vdots & \vdots & \ddots \end{bmatrix},$$

Our next step is to assemble the Global Mass Matrix. We produce it in a similar way as we did for B. The Element Mass Matrix is given by C;

$$\text{C}=\begin{bmatrix} \frac{1}{3} & \frac{1}{6} \\ \frac{1}{6} & \frac{1}{3} \end{bmatrix}.$$

We can then generate the Global Mass Matrix.

$$\text{D}=\begin{bmatrix} \frac{1}{3} & \frac{1}{6} & 0 & 0 & \dots \\ \frac{1}{6} & \frac{2}{3} & \frac{1}{6} & 0 & \dots \\ 0 & \frac{1}{6} & \frac{2}{3} & \frac{1}{6} & \dots \\ 0 & 0 & \frac{1}{6} & \frac{2}{3} & \dots \\ \vdots & \vdots & \vdots & \vdots & \ddots \end{bmatrix}.$$

Next, we assemble the Global Right-Hand side.

4.2. Right-Hand Side Function

Useful numerical simulations depend on appropriate right-hand-side function described as $f(c, d)$ in 8. We use two variations in our attempt to reproduce lab experimental results. We use three different types of functions to represent $f(c, d)$. Two of the variations are obtained from Mesuro and Scheel [8]. A claim of Mesuro and Scheel is that the threshold kinetics of [4] can be replaced by a continuous equation.

It must be noted that the system proposed by [8] is a slight variant of what our objective is, so quantitatively the results are not exactly the same as those produced in [8]. We are more interested in understanding if we can reproduce the same qualitative behavior expressed in [8].

In [8], Mesuro and Scheel do not assume the kinetics of the precipitate can be described by ordinary differential equation. A diffusion constant for the precipitate is also assigned but is small relative to the diffusion constants of the gaseous particles. Because the precipitate is assumed to diffuse and hence affect the threshold kinetics, we do expect the Liesegang ring formation in our simulation to be slower than that is observed in the Mesuro and Scheel Paper.

4.2.1. Method 1. In [8] a few alternative functions are given to replicate the behaviour of Equation 4. One of the alternatives that Mesuro and Scheel [8] provide is given as follows:

$$f_1(c, d) = -\beta(\frac{d}{\delta} - \alpha)e^{-\frac{d}{\delta}} - 1 + c. \tag{9}$$

There are certain conditions associated with the parameter values. For example, a stable solution requires $\beta > \alpha$. Using the same parameters, we reproduce the figure shown in [8].

4.2.2. Method 2- Counter-Diffusional Function. The counter-diffusional function is given as follows. This is one of the alternative functions given by Mesuro and Scheel.

$$f_2(c,d) = \alpha e^{-\beta d}(c + 0.75d(1-d)(d-\alpha)) \tag{10}$$

The same conditions about the parameter values conditions that apply to $f_1(c,d)$ also apply to $f_2(c,d)$.

The parameter values of α and β are varied to observe the change in results. According to Mesuro and Scheel, for the counter-diffusional function, $\alpha < \beta$ is needed for solution stability.

4.2.3. Method 3- Step Function. For our third alternative technique to solve for this particular problem is to solve for Equation 4 discretely at individual time steps and spatial nodes. We do not substitute Equation 4 with continuous functions as we did in Method 1 and Method 2. For every time-step and nodal point in the spatial domain, we check for the threshold conditions specified by Equation 5.

4.3. Computing the Monomer Ammonium Chloride

After selecting the desired function for our Right-Hand side we compute the Global Right-Hand side Matrix for all the spatial nodes n at time t using Equation 11.

$$z(a,b,c,d) = kab + f_i(c,d) \quad \forall i \in 1,2,3 \tag{11}$$

Now we have all the necessary tools to use the Crank-Nicholson method to solve for the monomer 'c'. To solve for the matrix C at the j^{th}, iteration we use the following scheme:

$$(D + \frac{h}{2}B)C^n = (D - \frac{h}{2}B)C^{n-1} + h(Z(t_n) + Z(t_{n-1}))/2 \tag{12}$$

where D is the Global Mass Matrix , B is the Global Stiffness Matrix, h is the mesh size in the spatial domain and C^n is the solution of the monomer at time t_n. $Z(t_n)$ is the Global Right-Hand side vector at time t_n.

As the time period has been partitioned as well, Equation 12 is solved for every iteration. Computationally this is very expensive and proved primarily difficult in running simulations with a very fine temporal partition and a long simulation time period. Once the matrix 'C' is solved for at the j^{th} iteration, we can then solve for the precipitate 'd'. Depending on the equation we have chosen from Section 4.2, the methodology for solving for the precipitate will also change accordingly.

4.4. Neumann Boundary Condition

The Neumann boundary conditions for the monomer, ammonium chloride is given by

$$\frac{\partial c(0,t)}{\partial x} = 0. \ \frac{\partial c(L,t)}{\partial x} = 0.$$

Since the partial derivative at both ends is equal to zero, we can treat the Neumann boundary condition through a to the first order approximation as follows

$$\frac{\partial c}{\partial x} \approx \frac{c_n - c_{n-1}}{h} \approx 0,$$

$$c_n - c_{n-1} \approx 0,$$

$$c_n \approx c_{n-1}.$$

This results in a modification to our finite element scheme. We now solve for all interior unknowns using the Crank-Nicholson method. Once the matrix is solved, we implement the Neumann boundary condition.

4.5. Spatial and Temporal Partitions

A finite element scheme is computationally expensive. Long time simulations rely on the stability of the solution. Δx, which is the spatial discretization (represented by h) in our model, was kept below 0.01 and Δt the temporal discretization was less than 0.1. We chose these numbers arbitrarily as long as they satisfy the following condition [9],

$$\Delta x^2 \leq \delta \Delta t$$

where δ is sufficiently small. In most of our simulations, $\delta \approx 0.001$. For saturated-vapor simulations the length of the tube was mostly 20 cm so the number of spatial nodes was 2000. Depending on the type of simulation, the total time of an experiment would vary between 300 to 500 seconds and have corresponding temporal nodes of 3000 to 5000 respectively.

4.6. Computing the Precipitate Ammonium Chloride

4.6.1. Using f_1 & f_2. For the equations derived from Mesuro and Scheel [8] f_1 and f_2 are continuous. A variety of numerical methods can be used to solve these ordinary differential equations. For f_1 and f_2, we solve for the precipitate using the second order Runge-Kutta for these ordinary differential equations.

Since the precipitate cannot diffuse we solve for the ODE using Runge-Kutta of order 2.

$$d(t_n, x) = \frac{1}{2}(k_1 + k_2)d(t_{n-1}, x) \tag{13}$$

where $k_1 = hf_{t_n}(c, d)$ and $k_2 = hf_{t_{n-1}}(c, d + k_1)$.

After the precipitate is solved for the j^{th} iteration , the precipitate 'd' is now used to solve for 'c' in the $(j+1)^{th}$ using the finite element scheme. This entire scheme is illustrated in Fig. 4.1.

4.6.2. USING f_3. For solving the precipitate using Equation 4, we check for the concentration of the monomer at every spatial node at every time iteration 'j' and see if it satisfies the threshold criterion.

The threshold criterion for homogeneous nucleation is said to be of the order of 10^{-2}. All of the simulations conducted assume a threshold in that range. Because the finite element scheme is one-dimension, in order to be more in tune with the physical reality of the dynamics of the model, we check for the threshold requirement based not on one node but rather on a neighborhood of points around the node of interest. If the average value of the neighborhood around the point is above the threshold then homogeneous nucleation takes place. Once the concentration of the monomer satisfies the threshold, homogeneous nucleation takes place. Once the precipitate forms at a particular point, the threshold drops exponentially. However, it is believed that there exists a minimum value of the threshold at the order of 10^{-3}. Fig. 2.1 shows the relationship between precipitate and threshold as

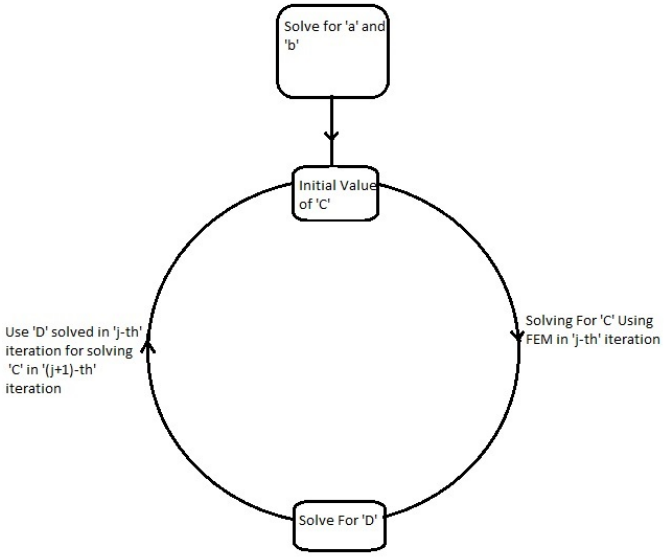

FIGURE 4.1. Numerical process in each iterative cycle.

modeled for this physical situation.

Once the threshold criterion is satisfied at one particular node, we have to develop a methodology for the conversion of the molecules in the gaseous state to the solid state. The amount of monomer converted into precipitate at a specific node is a hundred percent conversion that drops exponentially as we move away from the spatial node that has satisfied the threshold criterion. This process is executed for every node that has satisfied the threshold criterion. Once the precipitate is formed, the threshold drops as stated earlier and the same process is restarted for a new iteration.

CHAPTER 5

Results

For the coding of this entire process, MATLAB was used. We simulated the chemical reaction under different initial and boundary conditions. We categorize our simulations into two groups. In the first category, the initial conditions of both reactants is zero. The second category is the saturated-vapor tube where the initial condition of one of the reactants is a non-zero value. We then analyze the accuracy of our simulations to empirical data obtained from the lab. Other variations to our model include different boundary conditions of the reactants and the length of the tube.

5.1. Reproducing Results from Mesuro and Scheel

To check our code, we try to reproduce some of the results from Mesuro and Scheel [8]. Fig. 5.1 represents a saturated-vapor experiment with $a_o = 3$, $b_o = 0.55$ and $b_1 > 0$ and the length of the tube equal to $300cm$. The assumptions used for our model do vary slightly from [8] but what can observed that qualitatively and to a certain extent quantitatively the results are similar.

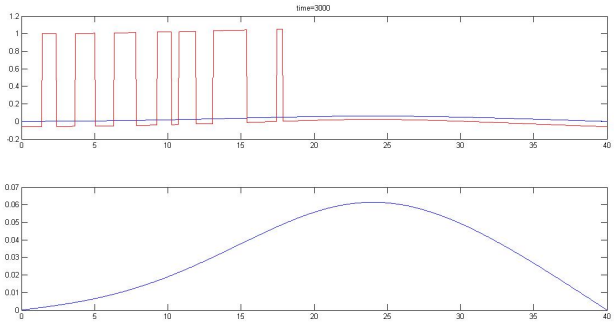

Figure 5.1. Saturated Vapor Simulation using continuous precipitory functions

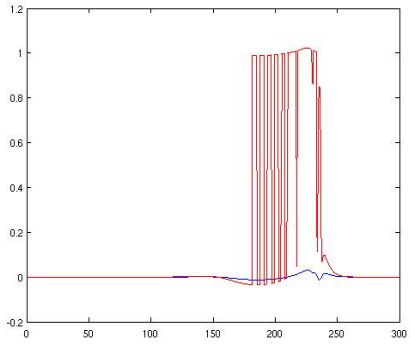

FIGURE 5.2. Counter-Diffusional Simulation using continuous precipitory finctions

Although in [8], the continuous precipitory function are not used for counter-diffusional experiments, we do use it and obtain the result in Fig. 5.2.

In both the above simulations, the precipitate and vapor ammonium chloride do achieve small negative values. Of course from a physical stand point it makes no sense but this error can be associated with the incorrect scaling of the continuous precipitory function which is referred to in [8].

5.2. Counter-Diffusional Results

5.2.1. Varying Boundary Conditions. As mentioned before in counter-diffusional experiments , the initial conditions of both reactants remains unchanged. What we do vary in counter-diffusional experiments are the boundary conditions. The boundary conditions play a very important role in precipitate formation because difference in vapor pressure at both ends determines the speed of the reaction front. The speed of the reaction front then determines the production of the monomer ammonium chloride and hence the production of the precipitate.

In Fig. 5.3 the initial point of contact is around 10 cm and then moves to the right. Because of the relative pressure difference of both hydrogen chloride and ammonia being

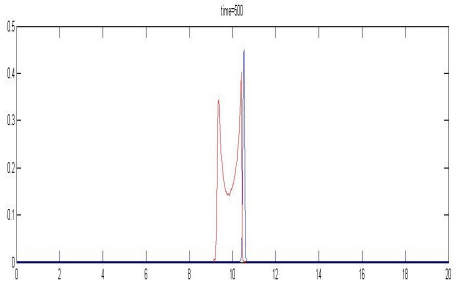

FIGURE 5.3. $a_o = 164$, $b_o = 103$,$b_1 = 0$,$a_1 = 0$

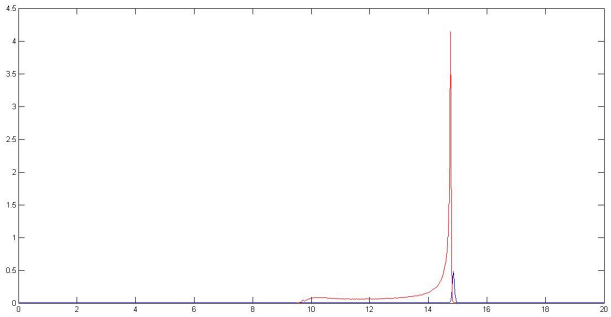

FIGURE 5.4. $a_o = 200$, $b_o = 50$,$b_1 = 0$,$a_1 = 0$

close to each other, the formation of precipitate reaches a type of equilibrium around the peak at 12 cm. With more simulation time we just see growth at the same point without much further spatial movement of the front.

In Fig. 5.4, the concentration ratio between the two reactants at the boundary is increased. Again, precipitate forms around the 10 cm mark but unlike in Fig. 5.3, the reaction front moves more to the right and equilibriates at a point further along the tube. The 'rings' might not be very apparent in Fig. 5.4, however if we take a closer zoom of the precipitate formation , we can see some interesting patterns.

After magnifying a portion of Fig. 5.4, we can some interesting concave-down patterns forming at regular intervals along the length of the tube in Fig. 5.5. This might not fit our

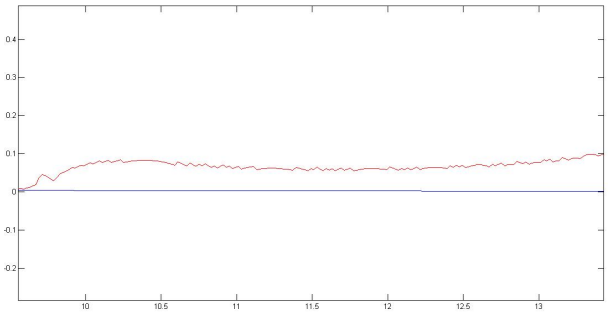

FIGURE 5.5. $a_o = 200$, $b_o = 50$,$b_1 = 0$,$a_1 = 0$

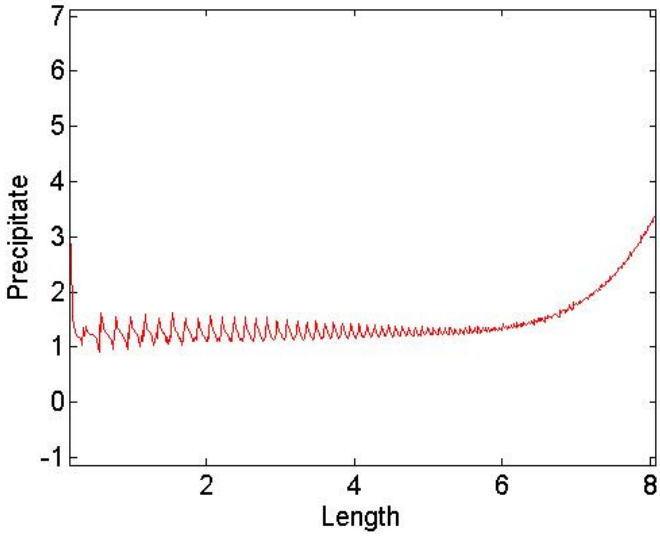

FIGURE 5.6. $k = 100$. $a_o = 164, b_o = 82, a_1 = 0$ and $b_1 = 20$.

visual interpretation of Liesegang rings but as far as concentration levels of the precipitate are concerned, this regular concave down pattern could be understood to be reflective of the visual interpretation of Liesegang rings.

5.3. Saturated-Vapor Simulations: Ammonia flooded tube

5.3.1. Varying Reaction Rate. In these simulation we vary the reaction rate between ammonia and hydrogen chloride, which is given by k in the mathematical model. There is debate over the exact value of the reaction rate, hence we vary it for three specific values over a large range.

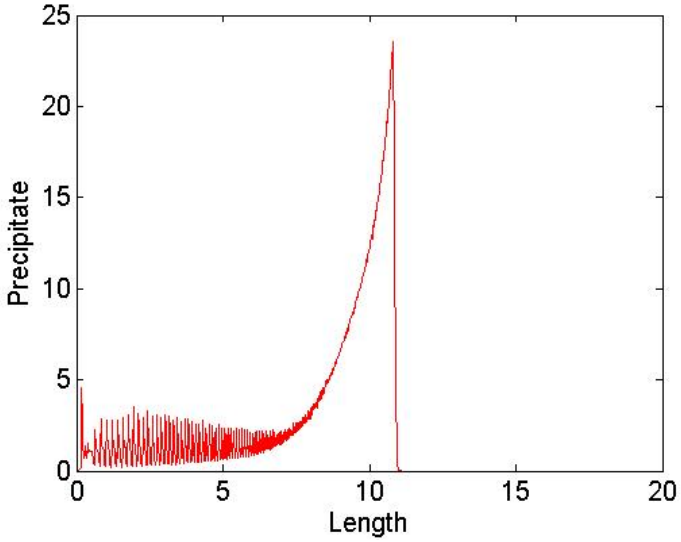

FIGURE 5.7. $k = 1000$. $a_o = 164, b_o = 82, a_1 = 0$ and $b_1 = 20$.

For the particular set of conditions represented in Fig. 5.6 we can get a very regular pattern as far as 'ring' formation is concerned. If we increase the reaction rate by a factor of 10 as represented in Fig. 5.7 we can see that we still have the same regular behavior but the amplitude of the precipitate is a lot higher. However this is not true for any set of parameter values or for reaction rates that are continuously increasing by a particular factor as we will see later in the case of the hydrogen chloride saturated tube.

5.3.2. VARYING BOUNDARY CONDITIONS. As identified before, the boundary condition determine the speed of the reaction front. In saturated-vapor simulations, the boundary condition of one of the reactants can be zero. In this case, the initial condition of ammonia is positive, hence $a_1 > 0$.

As expected, with the tube flooded by ammonia, the precipitate forms at the left hand side of the tube where hydrogen chloride is introduced at the boundary. As we are still introducing ammonia at the other end of the tube , we can see in Fig. 5.8 the reaction front stabilizing in the center of the tube. In the case the tube is flooded with ammonia with the $b_o = 0$. Hence, we can see precipitate forming throughout the tube.

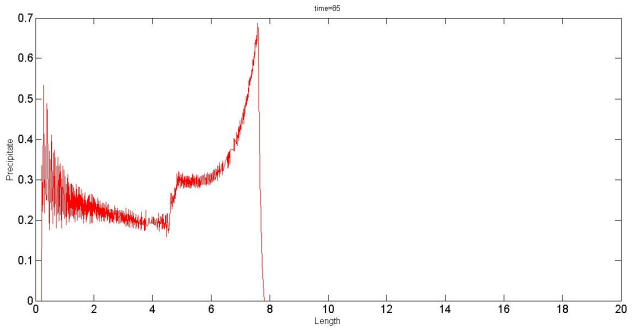

FIGURE 5.8. $k = 1000$. $a_o = 164, b_o = 103, a_1 = 0$ and $b_1 = 20$.

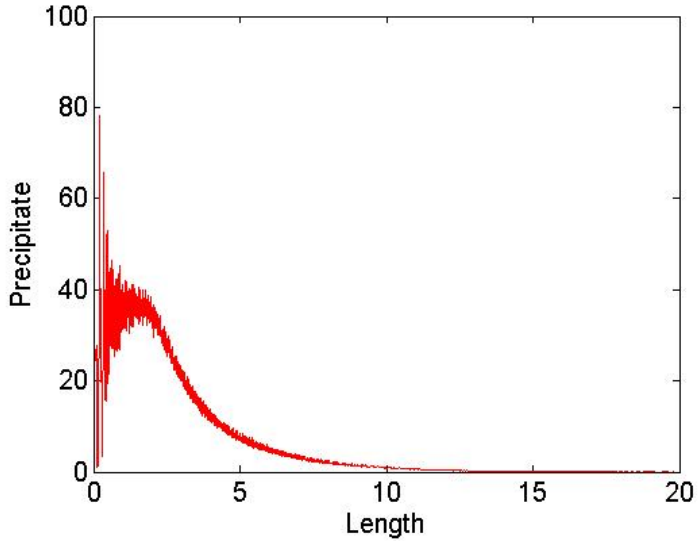

FIGURE 5.9. $k = 1000$. $a_o = 164, b_o = 0, a_1 = 0$ and $b_1 = 300$.

5.4. Saturated-Vapor Simulation: Hydrogen Chloride Flooded Tube

5.4.1. Varying Reaction rate. One point to note before looking at figures corresponding to the hydrogen chloride flooded tube is that for such simulation, we change the ends for ammonia and hydrogen chloride. So contrary to what was done in Section 5.3, ammonia is introduced at the left hand side of the tube rather than ammonia. Similarly however, as done previously in the ammonia saturated tube, we vary the reaction rate by factors of 10.

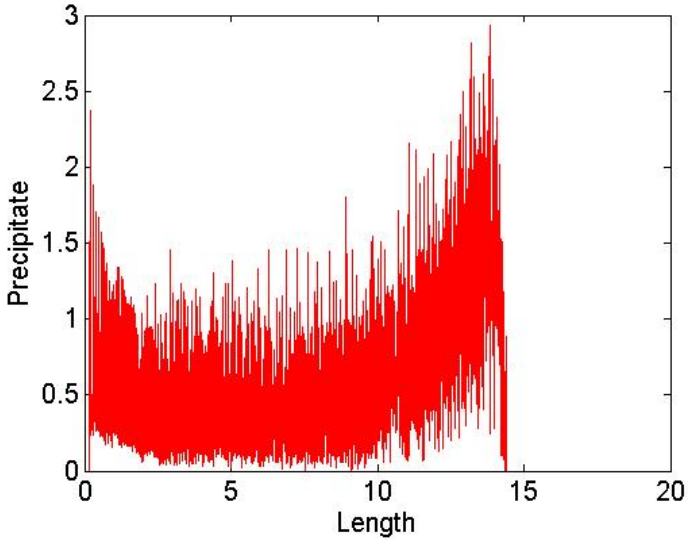

FIGURE 5.10. $k = 100$. $a_o = 10, b_o = 30, a_1 = 5$ and $b_1 = 0$.

In Fig. 5.10, for a different set of parameters we still have the same qualitative behavior but not as regular as in the case of the ammonia saturated tube. If we increase the reaction rate by a factor of 10 we again see the amplitude increase in Fig. 5.11 as compared to the precipitate value in Fig. 5.10. An interesting fact that arises however, is that if we increase the reaction rate by another factor of 10 we do not see the same level increase in precipitate value. There seems to be a certain limit to which the amplitude can increase as the reaction rate increases. The reaction rate in Fig. 5.12 is 10000.

This is somewhat interesting behaviour because we see the reaction rate starting to have a lower marginal affect on the precipitate as the reaction rate increases. Further analysis that we have not conducted would be of further interest to calculate the interval over which the effect of the reaction rate is the maximum.

5.4.2. VARYING BOUNDARY CONDITIONS. In these simulations, instead of flooding the tube with ammonia, we flood it hydrogen chloride. Different from previous figures provided, we interchange the reactants at each boundary. So now ammonia is introduced from left of the tube rather than the right in Fig. 5.13. If we now decrease the boundary and initial

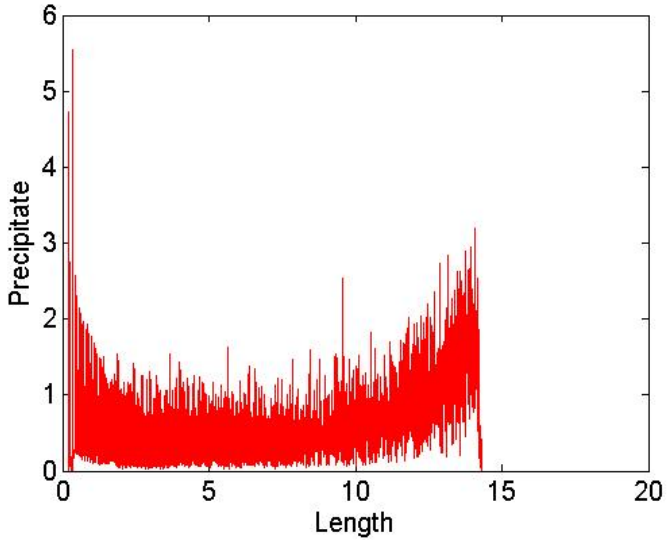

FIGURE 5.11. $k = 1000$. $a_o = 10, b_o = 30, a_1 = 5$ and $b_1 = 0$.

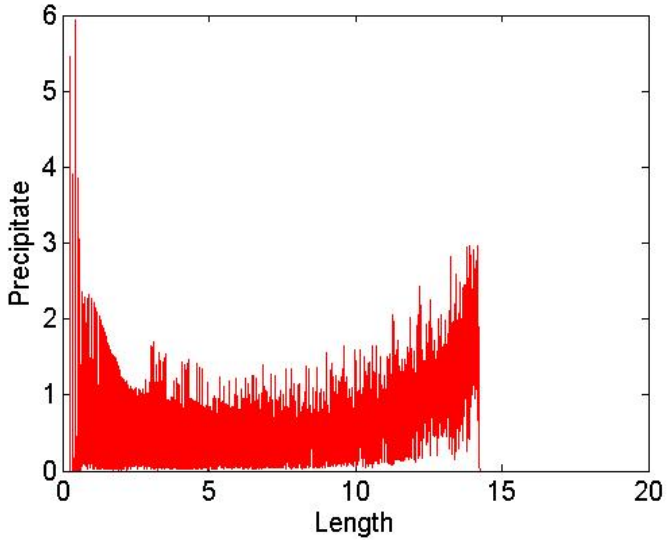

FIGURE 5.12. $k = 10000$. $a_o = 10, b_o = 30, a_1 = 5$ and $b_1 = 0$.

conditions by a factor of 10 we get Fig. 5.13. In Fig. 5.14, we increase the concentration of the initial and boundary conditions. That results in higher amplitudes of the precipitate as compared to Fig. 5.13.

5.4.3. VARYING THRESHOLD VALUE. The third most important parameter that we identified in the model was the threshold value. The experiments calculating the threshold value

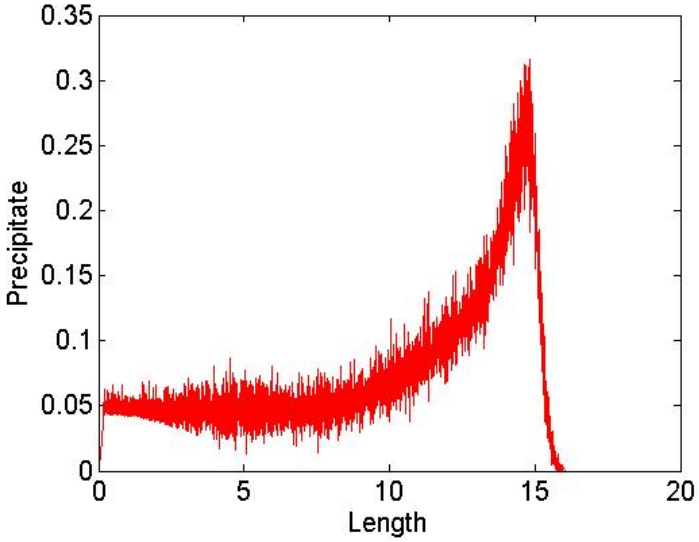

FIGURE 5.13. $k = 100$. $a_o = 1, b_o = 3, a_1 = 0.5$ and $b_1 = 0$ and homogeneous nucleation threshold 0.0123.

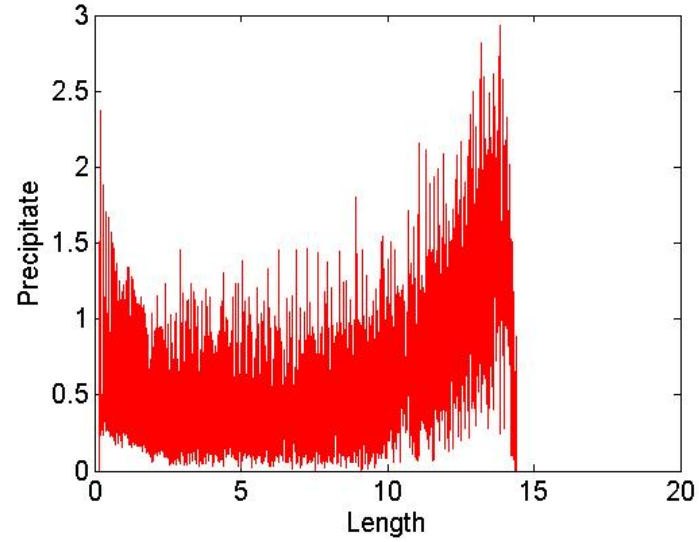

FIGURE 5.14. $k = 100$. $a_o = 1, b_o = 30, a_1 = 5$ and $b_1 = 0$ and homogeneous nucleation threshold 0.0123.

in [2] are fairly accurate and at this stage it might not make physical sense in our ability to change the threshold value. However, the results obtained from this hypothetical situation are interesting enough to list in this thesis for some future experiments where it could be possible to change the threshold requirement for precipitate formation. Compared to the

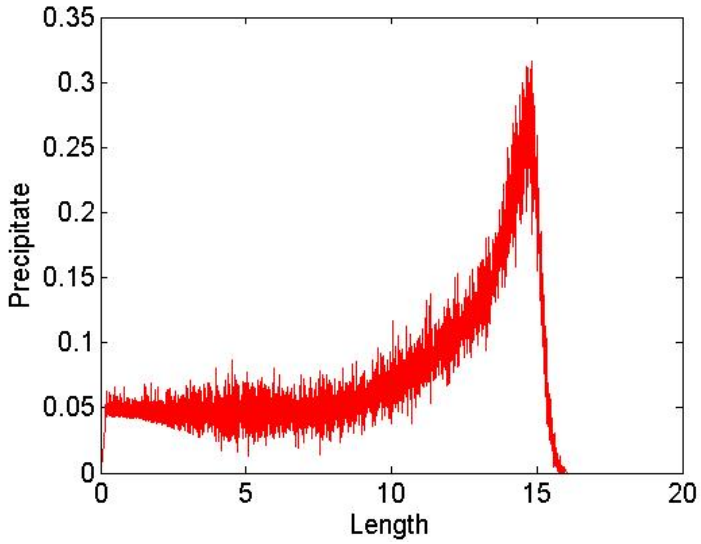

FIGURE 5.15. $k = 100$. $a_o = 1, b_o = 3, a_1 = 0.5$ and $b_1 = 0$ and homogeneous nucleation threshold 0.0123.

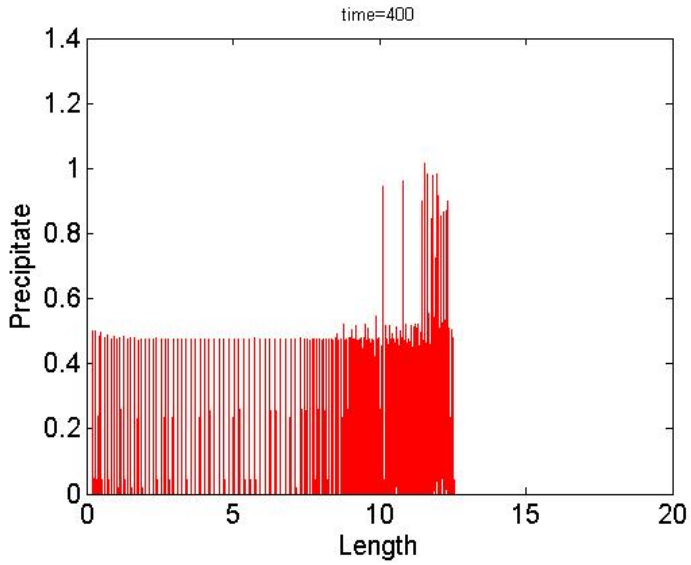

FIGURE 5.16. $k = 100$. $a_o = 1, b_o = 3, a_1 = 0.5$ and $b_1 = 0$ and homogeneous nucleation threshold 0.123.

parameter values of Fig. 5.15 we increase the threshold value for homogeneous nucleation and the lowest concentration value for precipitation to take place by a factor 10 in Fig. 5.16.

As can be seen from Fig. 5.16 we now have very distinct rings forming at discrete points. For the first time we don't have mathematically continuous formation of precipitate. The physical interpretation of this phenomenon can be understood by the fact that the threshold

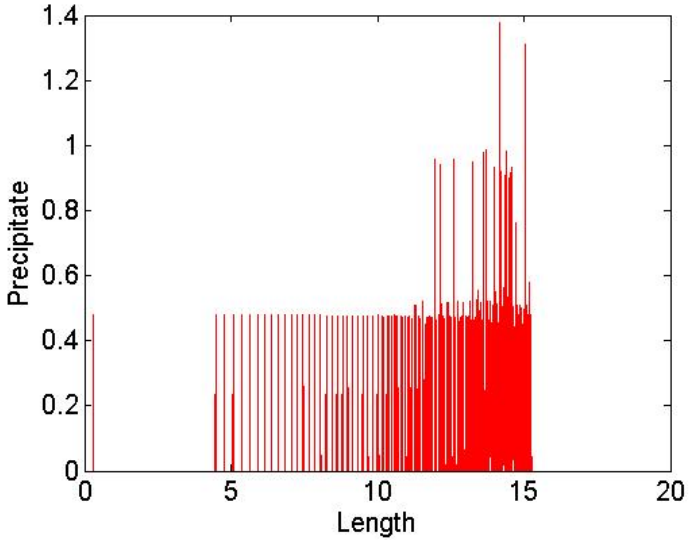

FIGURE 5.17. $k = 100$. $a_o = 1, b_o = 3, a_1 = 0.5$ and $b_1 = 0$ and homogeneous nucleation threshold 1.23.

value for precipitate formation is only reached at discrete points because the threshold value is high enough that after precipitate forms, the threshold value is only reached when the reaction front has moved a considerable distance. If we further increase the threshold value we get the results in Fig. 5.17.

In the case of Fig. 5.17, the threshold value is so high that it does not even reach that value for a good portion of time at the start of the experiment. Rings only start to form in a pattern similar to that in Fig. 5.16 towards the center of the tube when the reaction front starts to slow down.

CHAPTER 6

Analysis Lab of Data

One of the two claims made in [3], was that in a saturated-vapor tube the amplitude of the oscillations increases at the reaction front. The following graphs show the precipitate formed at the reaction front for different parameter values. From all simulation it is very clear that the amplitude of the oscillations increases at the front irrespective of the combination of parameter values.

6.1. Amplitude at Reaction Front

As mentioned before, one of the main claims of [3], was that the amplitude at the reaction front was increasing with time. We ran our simulation for various boundary and initial conditions. The length of the tube was varied and even the reaction rate between the reactants was adjusted. This was one claim that was substantiated and was very stable. Despite a different combination of parameter values, the amplitudes of the precipitate at the reaction front increased with time.

One issue that had to be dealt with was how to define the front. In our case, to calculate the amplitude of the precipitate at the front , we needed to have a precise definition for the front. Whenever the monomer increased above a threshold it converted to precipitate. So the only place which seemed logical to define as the 'front' was the moment where the monomer had the maximum value just before nucleation. So for each iteration, we calculated the maximum value of the monomer at each node before nucleation and then evaluated for the precipitate at that precise node after nucleation. The following graphs were obtained for various parameter values.

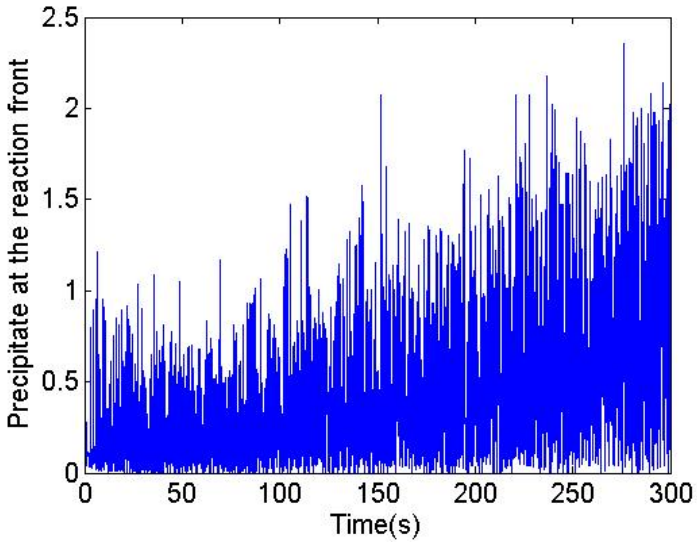

FIGURE 6.1. $k = 100$. $a_o = 10, b_o = 30, a_1 = 5$ and $b_1 = 0$.

6.1.1. VARYING REACTION RATE. Corresponding to Fig. 5.6 , Fig. 6.1 is the precipitate formed at the reaction front. In all three cases the amplitude at the reaction front increases with time. Each simulation is run for 300 seconds with reactions rates $k = 100, 1000, 10000$. One of the surprising observations on this case is that there is not a lot of difference in the precipitary values by changing the reaction rate too much. There is visible difference between Fig. 6.1 and Fig. 6.2 but not as much between Fig. 6.2 and Fig. 6.3. What it seems like is that after a particular value of the reaction rate 'k', the marginal affect of 'k' seems to rapidly reduce.

6.1.2. VARYING BOUNDARY CONDITIONS. In Fig. 6.4 instead of changing the reaction rate by factors of 10, we reduce the boundary and initial conditions by a factor of 10. Unlike in the case in which we varied the reaction rate by a factor of 10, in this case the precipitate at the reaction front does decrease by a factor of 10. Comparing Fig. 6.4 with Fig. 6.5 makes this point very clear.

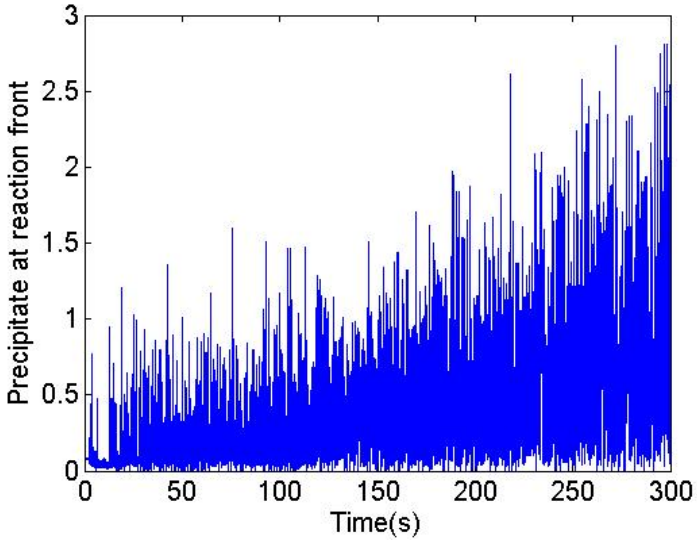

FIGURE 6.2. $k = 1000$. $a_o = 10, b_o = 30, a_1 = 5$ and $b_1 = 0$.

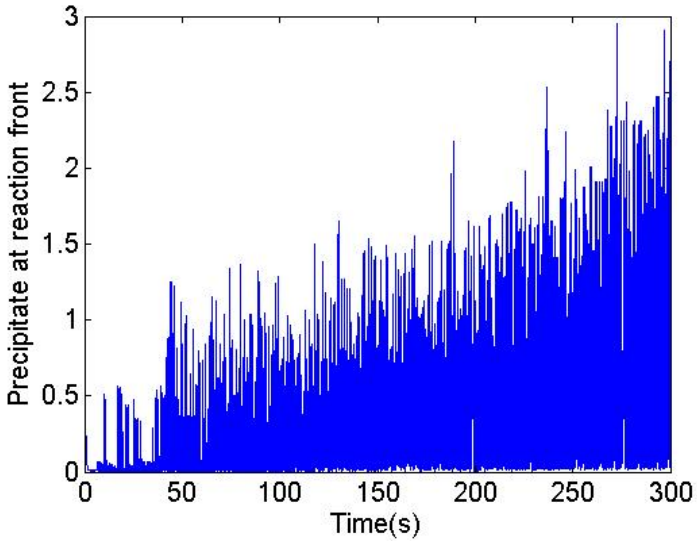

FIGURE 6.3. $k = 10000$. $a_o = 10, b_o = 30, a_1 = 5$ and $b_1 = 0$.

6.1.3. VARYING THRESHOLD. As mentioned before , the most interesting changes happened when the threshold value was adjusted. Corresponding to the figure presented in Section 5.4.3 the following figures represent the amplitude at the reaction front. With all the parameter values the same we increase the threshold values by a factor of 10 from Fig. 6.6-6.8. Immediately there is distinct behavior at the reaction front. We develop distinct and consistent patterns in Fig. 6.7 as well as in Fig. 6.8 compared to Fig. 6.6, where the pattern

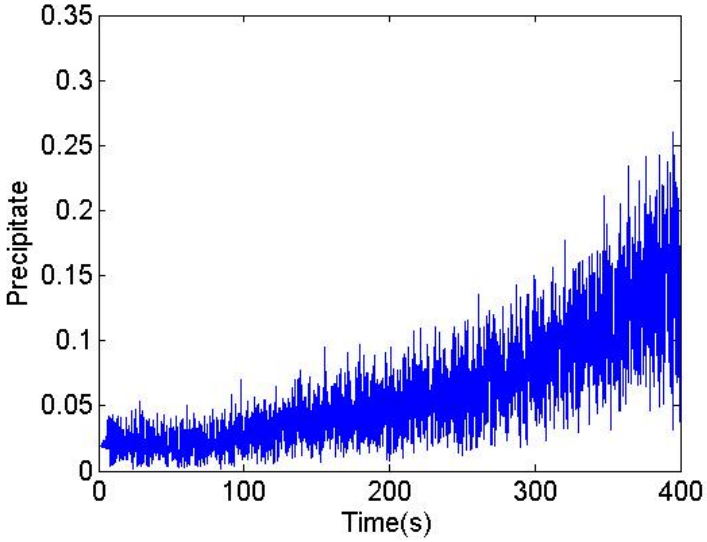

FIGURE 6.4. $k = 100$. $a_o = 1, b_o = 3, a_1 = 0.5$ and $b_1 = 0$.

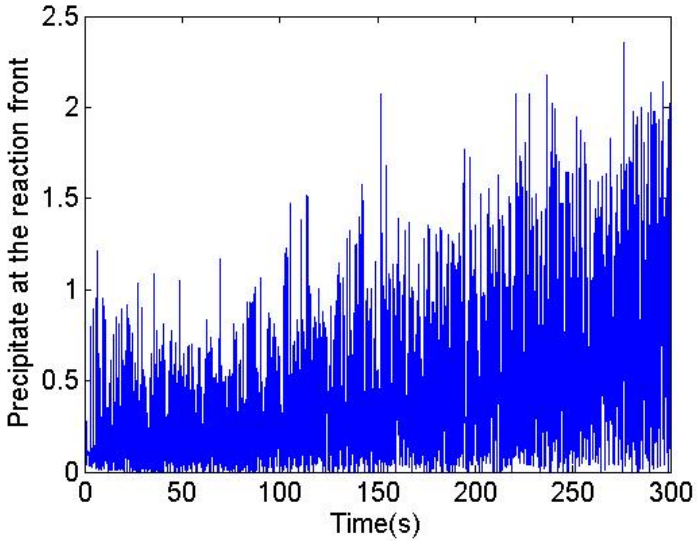

FIGURE 6.5. $k = 100$. $a_o = 10, b_o = 30, a_1 = 5$ and $b_1 = 0$.

is a lot less predictable. If we ignore the precipitate formation at the boundary, the first time any precipitate formed at the reaction happens after about 50 seconds in Fig. 6.8. As mentioned before in Section 5.4.3, the threshold value is so high that it never reaches it until it reaches the center of the tube where the reaction front velocity slows down and allows the supersaturation ration of the monomer ammonium chloride to reach the critical values for a phase transformation to take place.

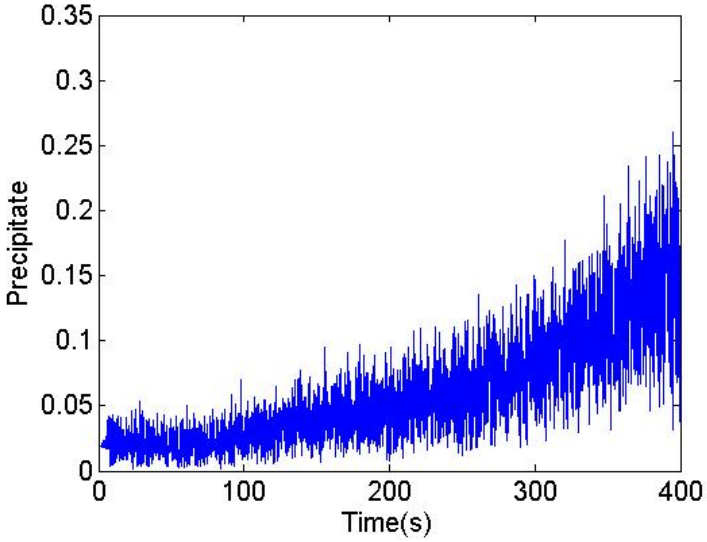

FIGURE 6.6. $k = 100$. $a_o = 1, b_o = 3, a_1 = 0.5$, $b_1 = 0$ and homogeneous nucleation= 0.0123

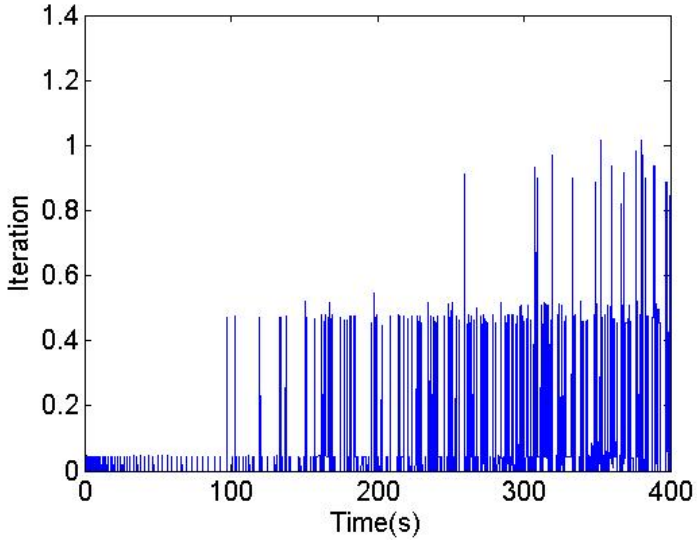

FIGURE 6.7. $k = 100$. $a_o = 1, b_o = 3, a_1 = 0.5$, $b_1 = 0$ and homogeneous nucleation= 0.123

6.2. Frequency of Oscillation at reaction Front

The other claim in [3] is that in a saturated-vapor tube the frequency of the precipitate formation at the reaction front decreases with time. Because the oscillations of the precipitate formation are not perfect sinusoidal graphs, the frequency can not be calculated by taking the inverse of the period. Instead we have to redefine frequency in a way that would give

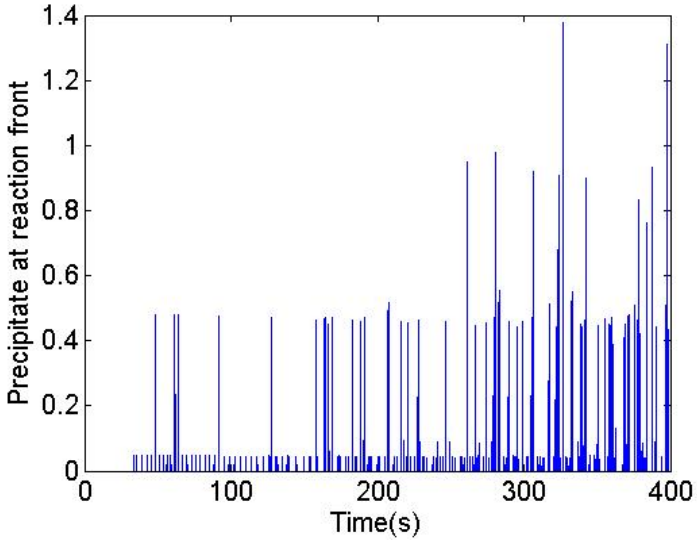

FIGURE 6.8. $k = 100$. $a_o = 1, b_o = 3, a_1 = 0.5$, $b_1 = 0$ and homogeneous nucleation= 1.23

us some level of understanding of the oscillatory behavior of that the reaction front always pattern formation.

After analyzing the data through this process, the information achieved was insufficient in providing the necessary perspective to understand the oscillatory behavior. The reason for that is the way we are solving for the precipitate. Because we solve for the precipitate at discrete intervals, the occurrence of extrema is very regular throughout the simulation. What gets damped in the information is the relative height of these peaks. So to gain more information , we use a proven claim from Section 6.1 about the simulation to calculate our re-defined 'frequency'. We use the claim in [3] that the amplitude of the oscillations increases with time. We define the frequency at the reaction front to be the reciprocal of the time required to exceed the previous maximum value at of the precipitate at the reaction front. As in the case, in the previous subsection we analyze the 'frequency' with different reaction rates, boundary conditions and threshold values for the hydrogen chloride saturated-vapor experiment.

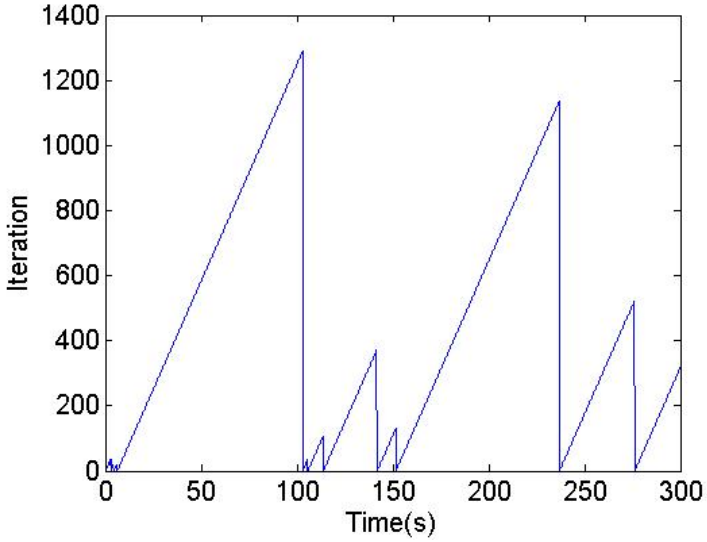

FIGURE 6.9. $k = 100$. $a_o = 10, b_o = 30, a_1 = 5$ and $b_1 = 0$.

6.2.1. VARYING REACTION RATE. To calculate the frequencies we change the reaction rate the same way as we did before. We change the reaction rate 'k' by factors of 10. We have values where $k = 100, 1000, 1000$. The way we defined the frequency, the graphs show the corresponding period value. The higher the triangle, the higher the period and hence lower the frequency.

With changing the reaction rate, the frequency seems to get more regular as the reaction rate is increased by a factor of ten. In all three cases as represented by Fig. 6.9-6.11, there seems to be a period in the beginning of the all the experiments where you have a high level of precipitate that takes a very long time to over come.

6.2.2. VARYING BOUNDARY CONDITION. If we change the corresponding boundary conditions by a factor of ten, it seems in the case with the higher boundary values (Fig. 6.13) there are larger wavelength , hence smaller frequencies. In both cases there seems to be a large formation of precipitate at the beginning of the simulation that is only over come after 100 seconds. In the case of Fig. 6.13 the frequency seems to be increasing with time rather than decreasing with time as suggested in [3].

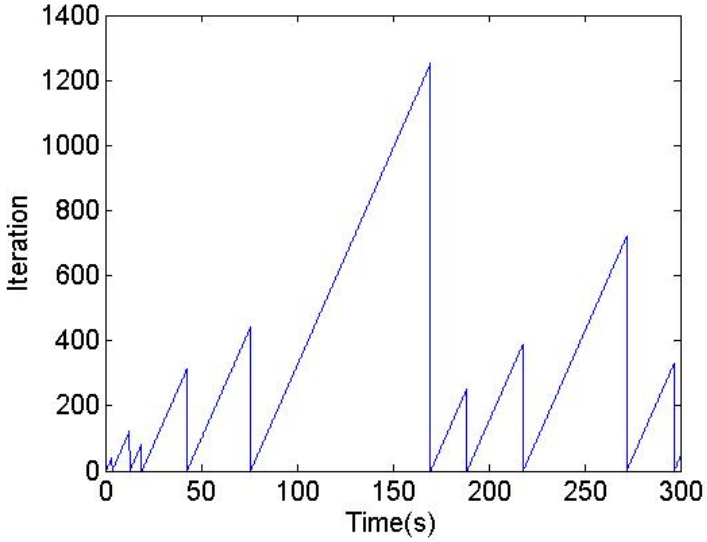

FIGURE 6.10. $k = 1000$. $a_o = 10, b_o = 30, a_1 = 5$ and $b_1 = 0$.

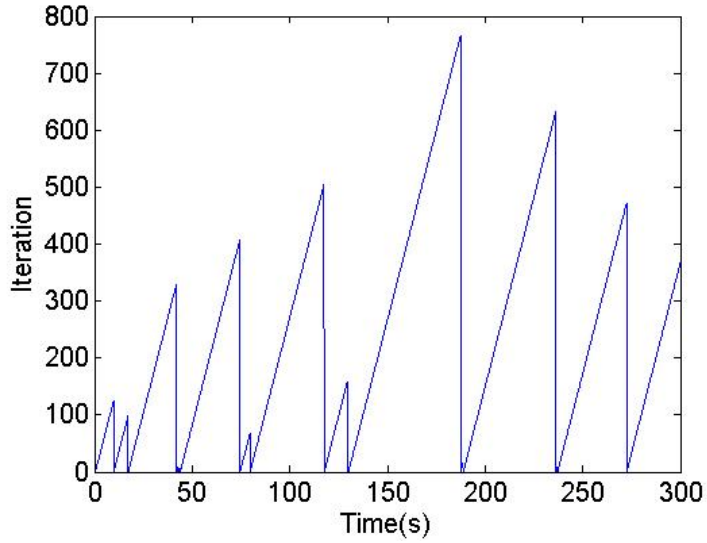

FIGURE 6.11. $k = 10000$. $a_o = 10, b_o = 30, a_1 = 5$ and $b_1 = 0$.

6.2.3. VARYING THRESHOLD. In this case we have the same set of parameters as in the previous case when we changed the threshold values. As can be seen in Fig. 6.14, it seems the frequency is increasing with time however in Fig. 6.15, the frequency seems to be decreasing with time. And if we increase the threshold even more, the frequency seems to decrease even more as represented by Fig. 6.16.

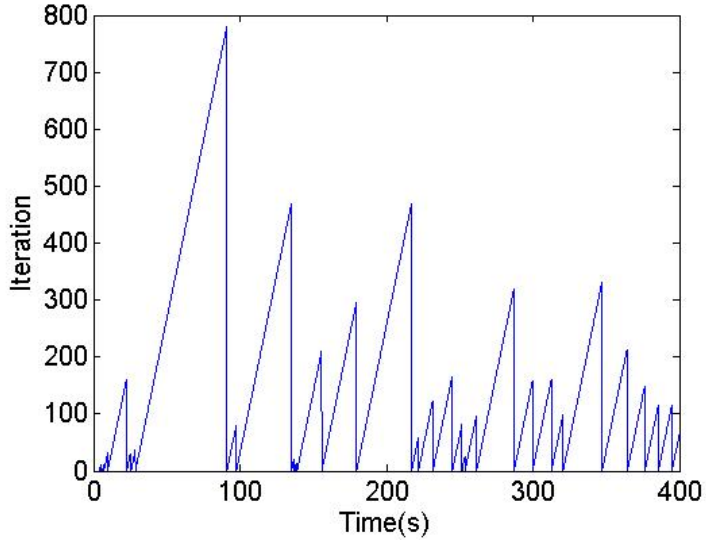

FIGURE 6.12. $k = 100$. $a_o = 1, b_o = 3, a_1 = 0.5$ and $b_1 = 0$.

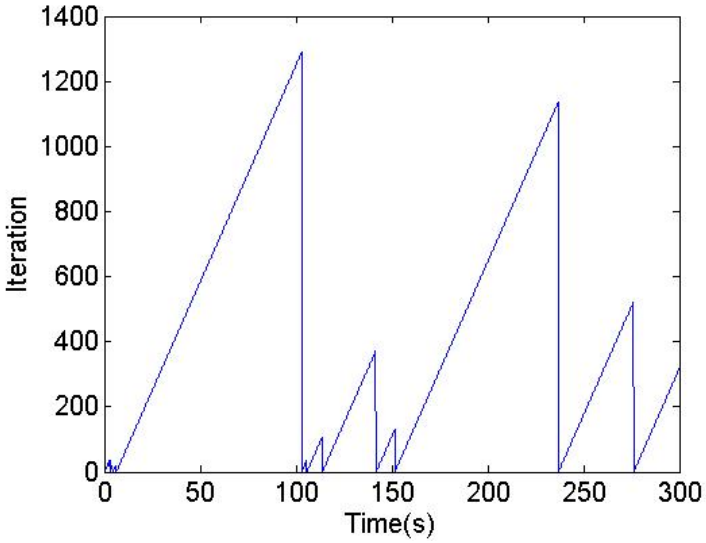

FIGURE 6.13. $k = 100$. $a_o = 10, b_o = 30, a_1 = 5$ and $b_1 = 0$.

In all three cases when we varied the threshold value, the precipitate, amplitude at the reaction front and the frequency seem to behave the same way in what was observed in lab experiments. From the distinct and consistent 'rings' obeying the spacing laws [3], there seems to be a set of parameter values that simulate actual lab experiment. More analysis on different parameter values and different chemical reactions could help us better understand the workings of our mathematical simulation. The conclusion that we can reach here , is

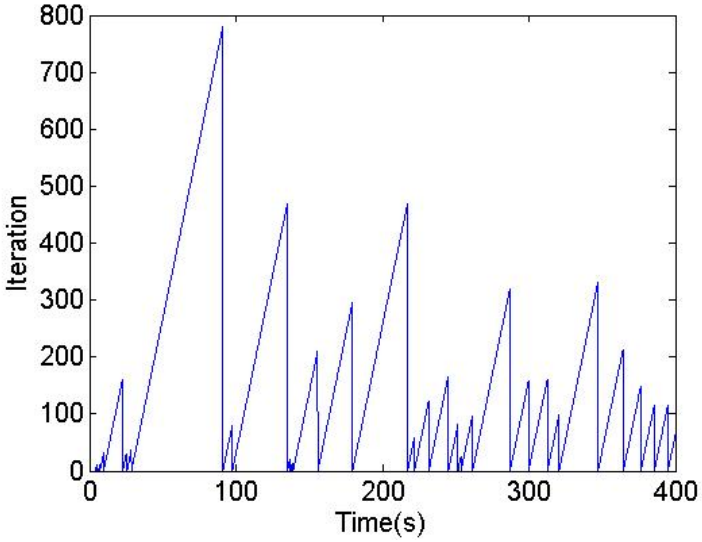

FIGURE 6.14. $k = 100$. $a_o = 1, b_o = 3, a_1 = 0.5$, $b_1 = 0$ and homogeneous nucleation = 0.0123

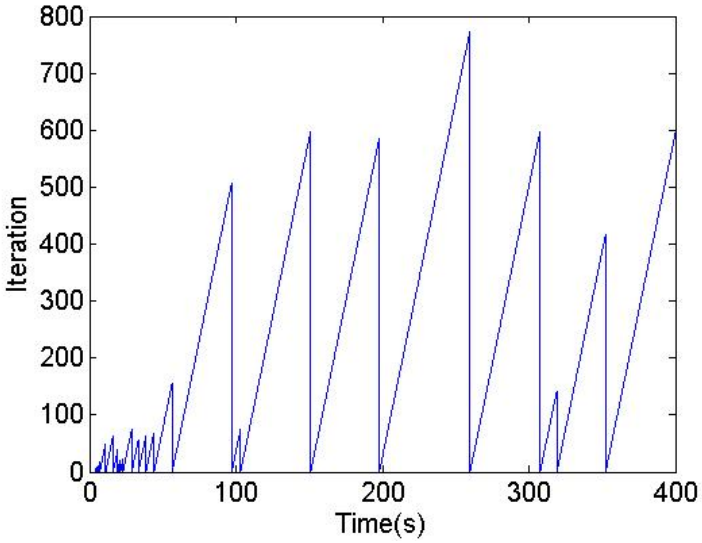

FIGURE 6.15. $k = 100$. $a_o = 1, b_o = 3, a_1 = 0.5$, $b_1 = 0$ and homogeneous nucleation = 0.123

that the most sensitive parameter is the threshold requirement. The boundary conditions also play a major role but the reaction rate is not as important factor in the development of Liesegang rings as was believed before running the mathematical simulation.

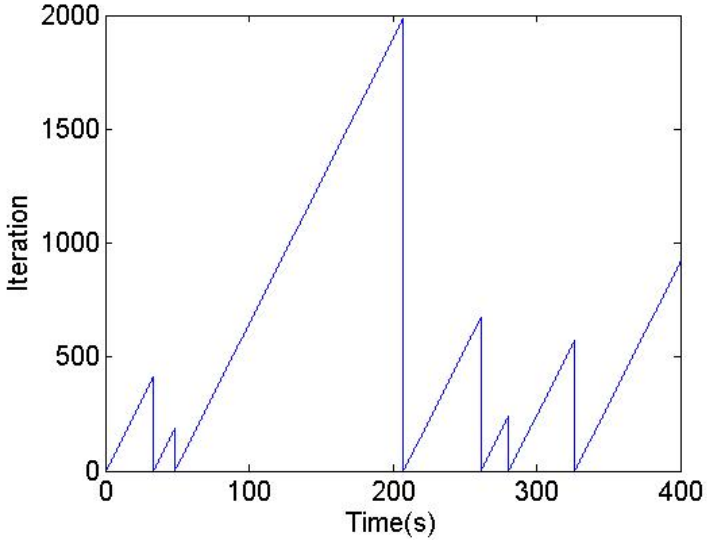

FIGURE 6.16. $k = 100$. $a_o = 1, b_o = 3, a_1 = 0.5$, $b_1 = 0$ and homogeneous nucleation = 1.23

6.3. CONCLUSION

There were two main claims in [3] regarding the precipitate formation at the reaction front. The first claim was that the amplitude of the precipitate formation was increasing with time. The second claim was that the frequency of the precipitate formation was decreasing with time. With regard to the first claim, under many different scenarios, our simulations also suggested that as time increases, the amplitude of the precipitate formed at the reaction front also increases. Our results for the second claim were a little more ambiguous. According to our redefined definition of frequency, under different conditions and parameter values, the frequency increased and decreased with time. The problem may lie with our definition of frequency but also with the fact that our model was a much simplified version of the real life experiments. For example, we assumed the system to be one-dimensional. Of course, in physical situations that is impossible. However, the biggest simplification that was not mentioned during the course of the thesis was the affect of the heat released when ammonia and hydrogen chloride react. The reaction between these two reactants is highly exothermic and hence a lot of heat is released. This induces convection currents that alter

the formation of Liesegang rings. In Fig. 1.1, it can be observed that the rings have not formed perpendicular to the base of the tube but rather at an angle. The slanting of the rings is believed to be the affect of the convection currents generated by the heat.

Future attempts to simulate the Liesegang ring process would not only involve converting the system into three dimensions but also take into consideration the thermal nature of the reaction in order to better understand and simulate this chemical reaction.

Bibliography

[1] Wikipedia, "Liesegang rings," 2014.

[2] S. Thompson and P. Shipman, "Patterns and oscillations: Extreme events in vapor-to-particle reaction zones,"

[3] T. Lenczycki, *Oscillations in gas-phase periodic precipitation patterns: The NH_3 - HCl Story*. Ms thesis, Colorado State University, Fort Collins, CO, 2003.

[4] J. Keller and S. Rubinow, "Recurrent precipitation and liesagang rings,"

[5] R. Dahlin, S. J, and L. Peters, "Aerosol formation in reacting gases: Theory and application to the anhydrous $nh_3 - hcl$ system," *AIChE*, vol. 27, pp. 404–418, 1981.

[6] M. Luria and B. Cohen, "Kinetics of gas to particle conversion in the nh_3-hcl system," *Atmospheric Environment*, vol. 14, pp. 665–670, 1980.

[7] J. Kirkby, J. Curtis, J. Almeida, E. Dunne, J. Duplissy, S. Ehrhart, and *et. al.*, "Role of sulphuric acid, ammonia, and galactic cosmic rays in atmospheric aerosol nucleation," *Nature*, vol. 476, pp. 429–433, 2011.

[8] R. Goh, S. Mesuro, and A. Scheel, "Coherent structures in reaction-diffusion models for precipitation,"

[9] C. Johnson, *Numerical Solution of Partial Differential Equations by the Finite Element Method*.